COMMUNICATION

High Dielectric Permittivity and Low Percolation Threshold in Nanocomposites Based on Poly(vinylidene fluoride) and Exfoliated Graphite Nanoplates

By *Fuan He, Sienting Lau, Helen Laiwa Chan,* and *Jintu Fan**

Ferroelectric polymers, such as poly(vinylidene fluoride) (PVDF), poly(vinylidene fluoride-*co*-trifluoroethylene) (P(VDF-TrFE)), and poly(vinylidene fluoride-trifluoroethylene-chlorofluoroethylene) (P(VDF-TrFE-CFE)) have great potential for applications in micro-electromechanical devices and high-charge storage capacitors.[1–3] In order to realize these applications, it is highly desirable to substantially improve the dielectric constants of such ferroelectric polymers.[4] Up to now, much work has focused on the preparation of 0–3-type composites based on polymers and ceramics of high dielectric constant, and the resultant composites usually possess a relatively high dielectric permittivity (about 100).[5–7] Nevertheless, the high volume fraction (> 50 vol%) of ceramics, which was necessary to achieve the high dielectric constants, presents a number of limitations, in terms of high weight, low flexibility, and poor mechanical performance, as a result of the weak matrix-filler bonding and agglomeration of ceramic nanoparticles.[8–10] Furthermore, most ceramics of high dielectric constant are lead-based, and potentially harmful to our health.

To overcome the limitations of ferroelectric polymer/ceramic composites, very promising work has been carried out recently based on percolation theory, in which a small volume fraction of some conductive filler was added to the polymer matrix to achieve a high dielectric constant, thus preserving the mechanical flexibility of the polymer.[4,9,11–16] For example, Dang et al.[9] fabricated a new poly(vinylidene fluoride)/carbon-nanotube composite, with a percolation threshold of 8 vol%, possessing a dielectric constant of 600 (the dielectric loss value, $\tan\delta$, is about 2) at 1000 Hz. For a P(VDF-TrFE-CFE)/carbon-nanotube system, the dielectric constant increased from 57 to 102 ($\tan\delta \approx 0.36$) at 100 Hz, by inclusion of only 2 wt% (1.2 vol%) carbon nanotubes.[4] A dielectric constant as high as 56 was observed in a PVDF/acetylene-black composite, when the acetylene-black concentration was in the neighborhood of the percolation threshold (about 1.3 vol%).[13] Recently, Panda et al.[14] reported that, for PVDF/Ni composites, a high effective dielectric constant of 2050 ($\tan\delta = 10$) at 100 Hz was observed near the percolation threshold of 27 vol%.

Along this line, in this communication, we propose a novel nanocomposite system consisting of poly(vinylidene fluoride) and exfoliated graphite nanoplates (PVDF/xGnPs). The xGnPs were selected as the conductive filler, because of their good electrical and thermal conductivity, high mechanical strength, and more importantly, large aspect ratio and unique layered structure with nanoscale thickness, which give advantages in the formation of a large number of parallel-board microcapacitors with low filler loading.[17–21] Moreover, functional groups, such as C–O–C, C–OH, and C=O, existing on the surface of graphite nanoplates, can promote the interaction between the PVDF and the graphite nanoplates, leading to good dispersion of xGnPs in the matrix.[19–21] It is well known that the homogenous dispersion of conductive fillers in a polymer matrix is a critical factor in achieving a high-performance nanocomposite.[4,6,9,11] Therefore, it was expected that a much lower volume fraction of xGnP in the PVDF/xGnP nanocomposite could result in a greater increase in dielectric permittivity.

xGnPs were obtained from subjecting natural graphite flakes to acidic intercalation, rapid thermal treatment, and ultrasonic powdering, in sequence (see **S1** in Supporting Information). Natural graphite flakes (see **S2** in Supporting Information), a naturally abundant and low-cost carbon-based material, are composed of parallel carbon layers. Carbon atoms within the graphite layers connect to each other to form six-member rings through strong covalent bonds, while the parallel carbon layers are joined together by weak van der Waals force. Such a structure makes it possible to intercalate some small molecules into the interlayer space of graphite. In the present study, natural graphite flakes were first converted to graphite intercalation compounds (GICs), through intercalation and chemical oxidation in the presence of concentrated H_2SO_4 and HNO_3. When heated at high temperatures, because of the volatilization of the mixed acid, the GICs could be expanded up to a few hundred times along the direction perpendicular to the carbon-layer plane of the intercalated graphite, so that expanded graphite (EG), which is a worm-like material (see the scanning electron microscopy (SEM) image, shown in Fig. 1a), could be obtained. It is also important to note that some functional groups could be introduced to the graphite during the preparation of the GICs and EG. After ultrasonic treatment, the graphite worms were fragmented into exfoliated graphite nanoplates with diameters of 0.5–25 μm and thicknesses of 20–60 nm (see **S3** in Supporting Information), as shown by the SEM image in Figure 1b.

[*] Prof. J. Fan, Dr. F. He
Institute of Textiles and Clothing
The Hong Kong Polytechnic University
Hung Hom, Kowloon, Hong Kong (China)
E-mail: tcfanjt@inet.polyu.edu.hk
Dr. S. Lau, Prof. H. L. Chan
Department of Applied Physics
and Materials Research Centre
The Hong Kong Polytechnic University
Hung Hom, Kowloon, Hong Kong (China)

DOI: 10.1002/adma.200801758

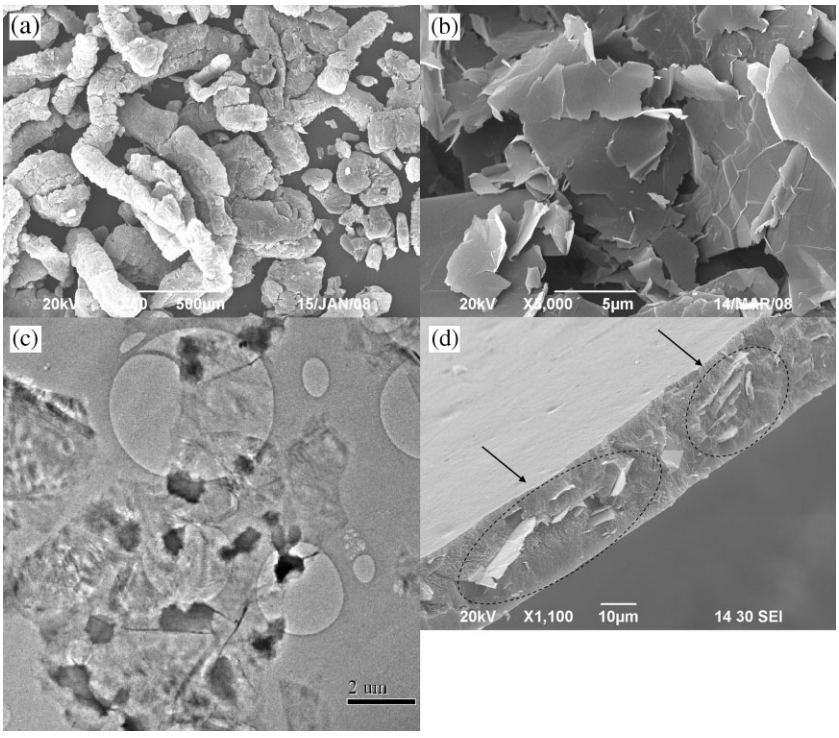

Figure 1. a) SEM image of EG. b) SEM image of xGnP. c) TEM image of PVDF/xGnP nanocomposite ($f_{xGnP} = 0.76$) prepared by solution casting. d) SEM image of fractured cross-section of PVDF/xGnP nanocomposite material ($f_{xGnP} = 0.76$). The dark arrows indicate the structures of microcapacitors.

Figure 1c shows the transmission electron microscopy (TEM) image of a PVDF/xGnP nanocomposite obtained from solution casting. Clearly, the graphite nanoplates were well dispersed in the PVDF matrix without any aggregation, which can be ascribed to specific interactions between the functional groups of the xGnPs and the $-CF_2-$ group of the PVDF. The interaction between the PVDF and xGnPs can also be confirmed by differential scanning calorimetry (DSC) and dynamic mechanical analysis (DMA) measurements (see **S5** and **S6** in Supporting Information). Furthermore, it should be noted that the graphite nanoplates tend to lie down inside the PVDF matrix. As a result, the faces of the xGnPs were parallel to the nanocomposite-film plate. During the hot-press process, several solution-cast films were stacked layer by layer in a ''sandwich'' form, and then pressed at 200 °C.[6] This promoted the formation of a larger number of microcapacitors in the nanocomposites. That is, the graphite nanoplates were parallel to each other, isolated by a polymer layer as a medium between the nanoplates, as shown in Figure 1d. We believe that the excellent dispersion of the xGnPs and the existence of many microcapacitors in the PVDF matrix are beneficial in achieving a high dielectric constant, but with low xGnP loading and dielectric loss.[11]

Elemental analysis of the xGnPs by energy dispersive X-ray analysis (EDAX, see **S4** in Supporting Information) showed an atomic ratio of carbon to oxygen of about 117:4. Compared with the results reported by Pan et al.,[20] the oxidation degree of graphite in this study was much lower, thus the good conductivity of the graphite was maintained. The oxidation of graphite can be further confirmed by the Fourier-transform infrared (FTIR) spectrum of the xGnPs in Figure 2. As can be seen, the band at 3433 cm^{-1} corresponds to the O–H stretching vibration. The presence of carboxyl functional groups is confirmed by the absorption at around 1800–1500 cm^{-1}.[19] The multiple bands in the 1400–1000 cm^{-1} region can be attributed to C–O–C and C–H vibrations.[21] A combination of EDAX and FTIR results indicates that, after the acidic intercalation and thermal treatment, some carbon double bonds were oxidized, resulting in the presence of oxygen-containing functional groups on the surface of the exfoliated graphite nanoplates. It is believed that these functional groups facilitate the interaction between the PVDF and xGnPs.[19]

PVDF/xGnP nanocomposites were prepared by a solution-cast and hot-press technique. The distribution of graphite nanoplates in the PVDF matrix is largely influenced by their dispersion state in the solvent. The good dispersion stability of the xGnPs in *N,N*-dimethylformamide (DMF) solvent and a DMF solution of PVDF is clearly evident from the photographic images (shown as insets a) and b) of Fig. 2), taken two weeks after the ultrasonic dispersion. The good dispersion stability of the xGnPs both in DMF solvent and PVDF solution may be attributed to the functionalization effect on the surfaces of graphite nanoplates.

The effective alternating-current (AC) conductivity as a function of the xGnP volume fraction at 1000 Hz is shown in Figure 3. It shows that the conductivity increases only slightly with the increase in xGnP volume fraction (f_{xGnP}), when the xGnP volume fraction is low. This is followed by an obvious insulator-to-conductor transition (known as the percolation

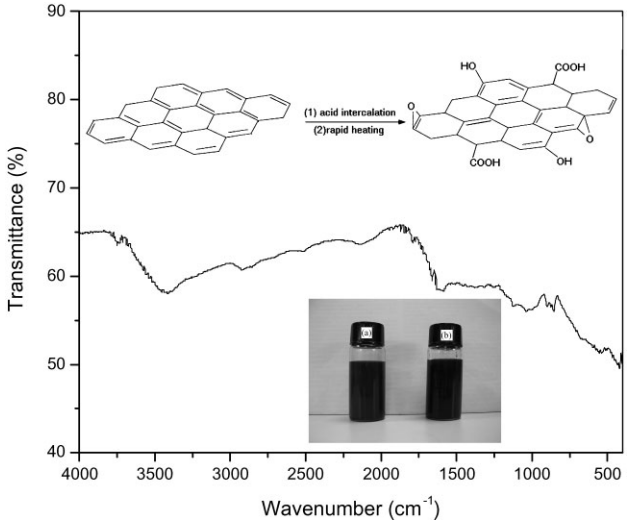

Figure 2. FTIR spectrum of xGnPs. The bottom right picture shows the dispersion stability of xGnPs in a) DMF solvent and b) PVDF solution, respectively.

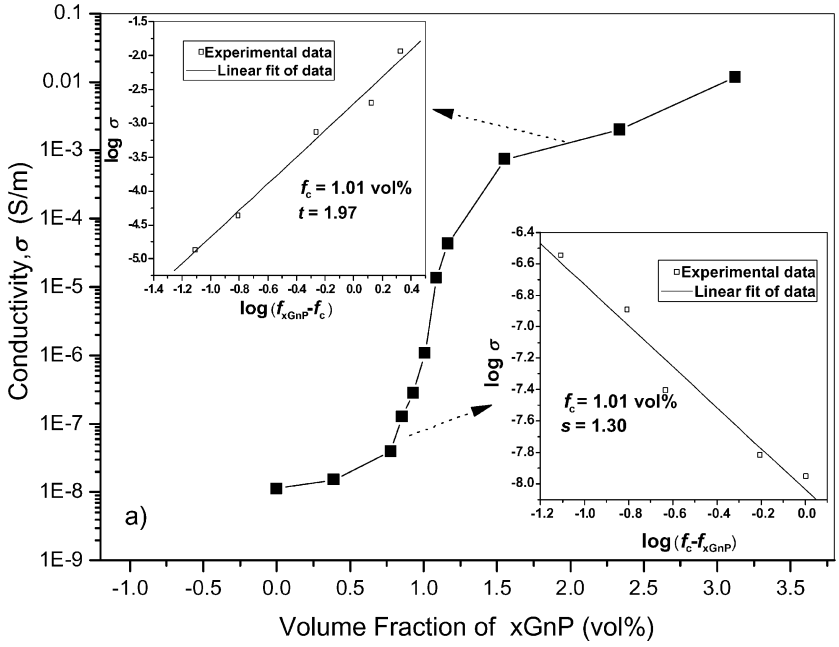

Figure 3. Effective conductivity of PVDF/xGnP nanocomposites as a function of xGnP volume fraction, measured at 1000 Hz and room temperature. The insets show the best fits of the conductivity to Equation 1.

transition) at $f_{xGnP} \approx 0.76$–1.55 vol%. The conductivity of the polymer/conductive-filler composites originates from two mechanisms: 1) Ohmic conduction, through direct contact of conductive fillers, and 2) non-Ohmic conduction, through the barrier-tunnelling effect between the conductive fillers separated by a polymer layer. The percolation transition can be seen as the transition from non-Ohmic conduction to Ohmic conduction, when the filler concentration approaches the percolation threshold.

The conductivity σ of the conductor-insulator composites near the percolation threshold can be predicted by the power laws in Equation 1a and b, as follows:

$$\sigma(f_{xGnP}) \propto (f_c - f_{xGnP})^{-s'} \quad \text{for } f_{xGnP} < f_c \tag{1a}$$

$$\sigma(f_{xGnP}) \propto (f_{xGnP} - f_c)^{t} \quad \text{for } f_{xGnP} > f_c \tag{1b}$$

In Equation 1, f_c is the percolation threshold, f_{xGnP} is the volume fraction of xGnP, and s' and t are the critical exponents in the insulating ($f_{xGnP} < f_c$) and conducting ($f_{xGnP} > f_c$) region, respectively. The best fits of the experimental conductivity values to the log–log plots of the power laws give $f_c = 1.01$ vol%, $t = 1.97$, and $s' = 1.30$ (see the insets in Fig. 3). The critical exponent in the conducting region, $t = 1.97$, is in agreement with the universal ones ($t_{un} \approx 1.6$–2). However, the critical exponent value in the insulating region, $s' = 1.30$, is higher than the universal value ($s_{un} \approx 0.8$–1), but close to that of PVDF/Ni composites.[14,22]

A giant increase in the dielectric constant near the percolation threshold can be obtained, as predicted by the percolation theory. As shown in Figure 4, the dielectric constant improved dramatically, and up to more than 200 when $f_{xGnP} = 1.01$ vol%, which is 20 times larger than that of pure PVDF (about 10). As far as the dielectric loss is concerned, an abrupt increase was observed near the percolation threshold (see the bottom right inset of Fig. 4), which is expected due to the formation of conductive paths within the nanocomposites. At $f_{xGnP} = 1.01$ vol%, the dielectric loss was 0.48, which is still acceptable for applications such as high-charge storage capacitors. As f_{xGnP} increased beyond the percolation threshold, the dielectric constant of the PVDF/xGnP nanocomposites continued to rise, to an exceptionally high value of about 4.5×10^7 at 1000 Hz,[23] although at this point the dielectric loss was also high (229). This high-dielectric-permittivity

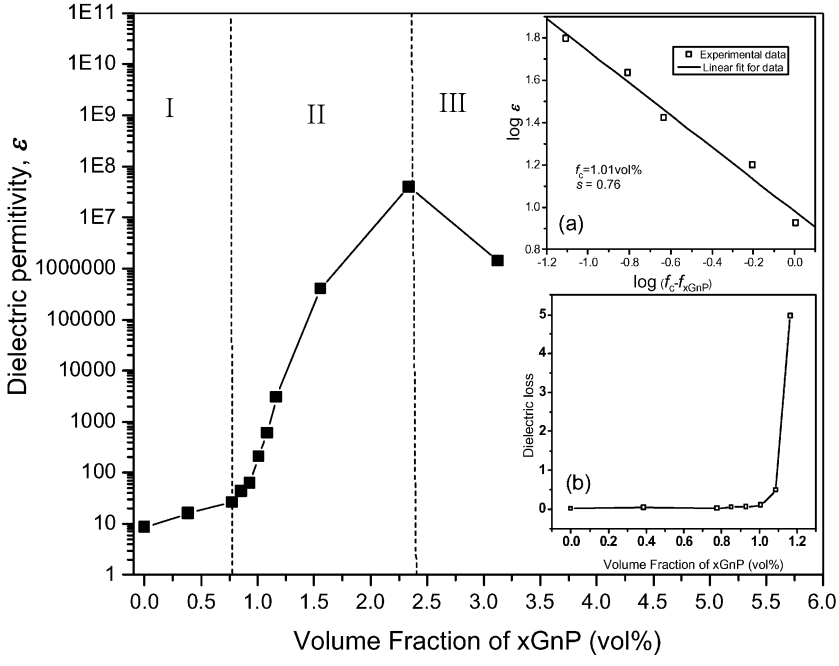

Figure 4. Effective dielectric constant of the PVDF/xGnP nanocomposites as a function of the xGnP volume fraction, measured at 1000 Hz and room temperature. Inset a) shows the best fits of the conductivity to Equation 2. Inset b) shows the loss tangent of PVDF/xGnP nanocomposites as a function of xGnP volume fraction.

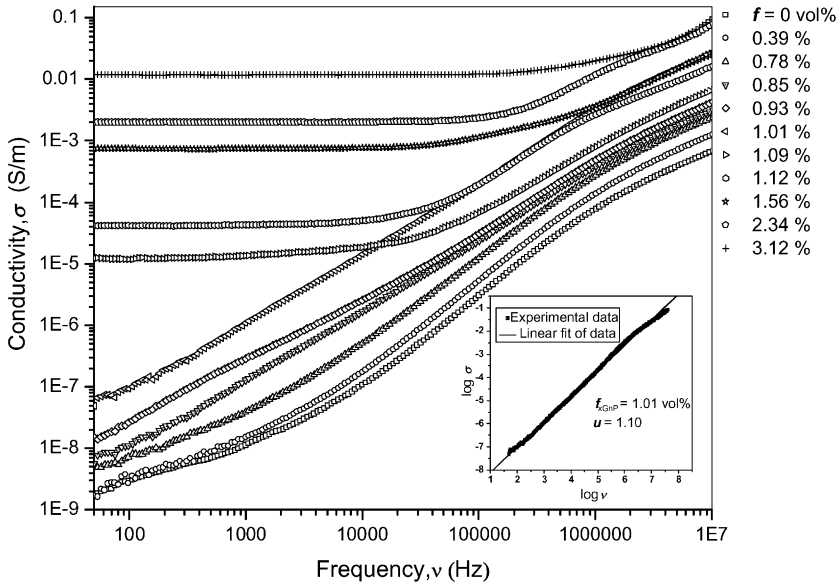

Figure 5. Dependence of effective conductivities on the frequency for PVDF/xGnP nanocomposites at room temperature. The best fit of the effective conductivity for $f_{xGnP} = 1.01$ vol% to Equation 3 is shown in the inset.

and high-dielectric-loss nanocomposite is highly beneficial in applications such as electromagnetic-wave absorption. When the xGnP concentration is near the percolation threshold, the dielectric constant (ε) can be characterized by the percolation-theory power law in Equation 2, as follows:

$$\varepsilon(f_{xGnP}) \propto (f_c - f_{xGnP})^{-s} \quad \text{for } f_{xGnP} < f_c \qquad (2)$$

In Equation 2, $f_c = 1.01$ vol% and $s = 0.76$ (see the top right inset of Fig. 4).

Figure 5 shows the conductivity of the PVDF/xGnP nanocomposites as a function of frequency with different xGnP loadings. When $f_{xGnP} < f_c$, the conductivity increases almost linearly with the increase of frequency; when $f_{xGnP} > f_c$, the conductivity values are much greater than those for $f_{xGnP} < f_c$, and are almost independent of the change of frequency within a low-frequency range. The percolation-threshold power law is described in Equation 3:

$$\sigma \propto \omega^u, \quad \varepsilon \propto \omega^{u-1} \quad \text{as } f_{xGnP} \to f_c \qquad (3)$$

In Equation 3, $\omega = 2\pi\nu$, where ν is the frequency, and u is the corresponding critical exponent. The experimental data for the nanocomposite with $f_c = 1.01$ vol% give $u = 1.10$, which is larger than the calculated value: $u = \frac{t}{(s+t)} = \frac{1.97}{(0.76+1.79)} = 0.72$.[24] A similar result has been reported in polyimide/silver composites.[25]

Figure 6 shows the dielectric permittivity of the PVDF/xGnP nanocomposites as a function of frequency with different xGnP loadings. As can be seen, when $f_{xGnP} < f_c$, the dielectric constant decreases very slowly with the increase of frequency; when $f_{xGnP} \geq f_c$, the dielectric constant reduces sharply in the low-frequency range, followed by a gradual decrease in the high-frequency range.

The dielectric properties of the novel PVDF/xGnP nanocomposites are compared with those of PVDF/conductive-filler composites reported in the literatures (see **S7** in Supporting Information). As can be seen, 1) A low percolation threshold is important in maintaining the mechanical flexibility of PVDF. The percolation threshold of PVDF/xGnP nanocomposites, $f_c = 1.01$ vol%, is much lower than the lowest percolation threshold of PVDF/conductive-filler composites reported previously. Our experimental findings agree well with the recent theoretical prediction by Xie et al.,[26] who predicted that planar conductive fillers with extremely high aspect ratios can significantly enhance the conductivity and dielectric constant of composites at a very small percolation transition. 2) In the percolative stage ($f_{xGnP} = f_c = 1.01$ vol%), the dielectric constant of PVDF/xGnP nanocomposites at 100 Hz is near 2700, which is significantly higher than that of the PVDF/conductive-filler composites previously reported, and is three

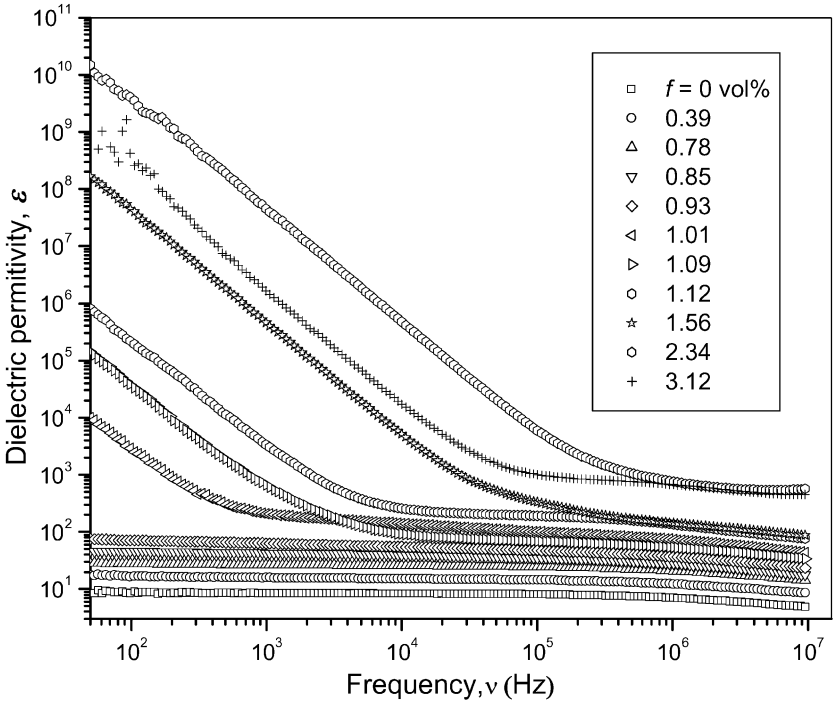

Figure 6. Dependence of dielectric constants on the frequency for PVDF/xGnP nanocomposites at room temperature.

times that of a poly(vinylidene fluoride)/carbon-nanotubes composite ($f_{MWNT} = f_c = 8$ vol%).[9]

The significant increment in dielectric constant of PVDF/xGnP nanocomposites can be mainly attributed to the homogenous dispersion of xGnPs in the PVDF polymer matrix and a gradual formation of the microcapacitor networks in the PVDF/xGnP nanocomposites as the xGnP content increases.[9,12] The evolution process of the dielectric constant in PVDF/xGnP nanocomposites with the change of xGnP content can be divided into three stages (I, II, and III). Initially, as shown in part I of Figure 4, when a small amount of xGnPs is incorporated into the PVDF matrix, some microcapacitance structures are formed, resulting in a slight increase of dielectric constant relative to that of pure PVDF. As the xGnP content is further increased, the dielectric constant gradually rises. Up to the percolation threshold (see part II of Figure 4), there are many conductive graphite nanoplates isolated by very thin dielectric insulating-polymer layers within the nanocomposites, forming lots of microcapacitors, which leads to a very high dielectric constant. Then, beyond the percolation threshold, the dielectric constant of the PVDF/xGnPs keeps on rising, because the graphite nanoplates are still wrapped by a thin layer of polymer matrix, if they are well dispersed. As the xGnP content increases to 3.12 vol%, the dielectric constant decreases (see part III of Figure 4), due to the formation of a significant conductive network, and the resultant leakage current within the nanocomposite.[15]

In addition, Maxwell–Wagner–Sillars (MWS) polarization for heterogeneous systems also plays a very important role in improving the dielectric constant.[9] The MWS effect, which is associated with the entrapment of free charges between the insulator/conductor interfaces, can be characterized by the frequency dependence of the dielectric constant in the low-frequency range. For the PVDF/xGnP nanocomposites, the dielectric constant is almost independent of frequency when $f_{xGnP} < f_c$, indicating that there is no plentiful accumulation of interfacial charges inside the nanocomposites. As soon as the percolation process takes place, a sudden increase in dielectric constant at low frequencies can be observed. This means that there were many xGnPs separated by very thin dielectric PVDF layers. Thus, a lot of charges were blocked at the interfaces between the filler and polymer matrix, owing to the MWS effect, which makes a remarkable contribution to the increment of the dielectric permittivity in the low-frequency range. However, when the frequency was over 10^5 Hz, the dielectric permittivity of the composites was dominated by the microcapacitance-structure model (frequency-independent), so that it is maintained at a stable value of about 100, which is still much larger than that of pure PVDF.

In conclusion, a novel PVDF/xGnP nanocomposite was successfully fabricated by a solution-cast and hot-press method. It was found that the homogenous dispersion of xGnPs in the PVDF matrix could significantly improve the dielectric constant of a PVDF/xGnP nanocomposite with an extremely low percolation threshold. A high dielectric constant of more than 200 and 2700 could be obtained for the PVDF/xGnP nanocomposite near the percolation threshold (1.01 vol%) at 1000 and 100 Hz, respectively, which is 20 and 270 times higher than that of a PVDF matrix. When above the percolation threshold, the dielectric constant continued to increase, and the maximum value was as high as 4.5×10^7, with a high dielectric loss of 229 at 1000 Hz (2.34 vol%). The giant increment in the dielectric permittivity can be explained by the combination of the microcapacitance-structure model and the MWS effect. These flexible PVDF/xGnP nanocomposites with such high dielectric performance are potential materials for practical applications in high-charge storage capacitors and electromagnetic-wave absorption.

Experimental

The preparation of the xGnPs was described in the main text. PVDF/xGnP nanocomposites were prepared as follows: a desired amount of xGnPs was first ultrasonically dispersed in 200 mL of *N*,*N*-dimethylformamide (DMF) for 1 h. Then, PVDF was added into the xGnP suspension. After stirring for 30 min at 80 °C, and ultrasonicating for another 2 h, the mixture was poured onto a glass plate to form a thin film, and dried at 70 °C for 3 days. Samples for testing were made by hot-pressing several solution-cast films stacked together at 200 °C, as described by Arbatti et al. [6]. The dielectric properties of the samples were measured using an Agilent 4294 A impedance analyzer in the frequency range of 50–10^7 Hz at room temperature. SEM (JEOL Model, JSM-6490) and TEM (JEOL Model, JEM-2010) were employed to observe the microscopic structures of the xGnPs and PVDF/xGnP nanocomposites.

Acknowledgements

The authors would like to acknowledge the funding support of Research Grant Council of HKSAR in the form of a CERG project (PolyU 5164/06E) and the funding support of Hong Kong Polytechnic University in the form of a Niche Area Project (1-BB82). Supporting Information is available online from Wiley InterScience or from the authors.

Received: June 24, 2008
Revised: August 5, 2008
Published online: December 12, 2008

[1] Q. M. Zhang, H. F. Li, M. Poh, H. S. Xu, Z. Y. Cheng, F. Xia, C. Huang, *Nature* **2002**, *419*, 284.
[2] Q. M. Zhang, V. Bharti, X. Zhao, *Science* **1998**, *280*, 2101.
[3] C. G. Naber, C. Tanase, P. W. M. Blom, G. H. Gelinck, A. W. Marsman, F. J. Touwslager, S. Setayesh, D. M. de Leeuw, *Nat. Mater.* **2005**, *4*, 205.
[4] S. H. Zhang, N. Y. Zhang, C. Huang, K. L. Ren, Q. M. Zhang, *Adv. Mater.* **2005**, *17*, 1897.
[5] Z. M. Dang, Y. Shen, C. W. Nan, *Appl. Phys. Lett.* **2002**, *81*, 4814.
[6] M. Arbatti, X. B. Shan, Z. Y. Chen, *Adv. Mater.* **2005**, *19*, 1369.
[7] P. Kim, S. C. Jones, C. W. Hotchkiss, B. Kippelen, S. R. Marder, S. R. Marder, J. W. Perry, *Adv. Mater.* **2007**, *19*, 1001.
[8] Y. Shen, Y. H. Lin, M. Li, C. W. Nan, *Adv. Mater.* **2007**, *19*, 1418.
[9] Z. M. Dang, L. Wang, Y. Yin, Q. Zhang, Q. Q. Lei, *Adv. Mater.* **2007**, *19*, 852.
[10] L. Wang, Z. M. Dang, *Appl. Phys. Lett.* **2005**, *87*, 040923.
[11] T. Wei, C. Q. Jin, W. Zhong, J. M. Liu, *Appl. Phys. Lett.* **2007**, *91*, 222907.
[12] Z. M. Dang, J. P. Wu, H. P. Xu, S. H. Yao, M. J. Jiang, J. B. Bai, *Appl. Phys. Lett.* **2007**, *91*, 072912.
[13] Q. Chen, P. Y. Du, L. Jin, W. J. Weng, G. R. Han, *Appl. Phys. Lett.* **2007**, *91*, 022912.
[14] M. Panda, P. V. Srinivas, A. K. Thakur, *Appl. Phys. Lett.* **2008**, *92*, 132905.
[15] Y. J. Li, W. Xu, J. Q. Feng, Z. M. Dang, *Appl. Phys. Lett.* **2006**, *89*, 072902.
[16] Y. Shen, Z. Yue, M. Li, C.-W. Nan, *Adv. Funct. Mater.* **2005**, *15*, 1100.

[17] S. Stankovich, D. A. Dikin, G. H. B. Dommett, K. M. Kohlhaas, E. J. Zimney, R. C. Piner, S. T. Nguyen, R. S. Ruoff, *Nature* **2006**, *442*, 282.
[18] J. J. Mack, L. M. Viculis, A. Ali, R. Luoh, G. L. Yang, H. T. Hahn, F. K. Ko, R. B. Kaner, *Adv. Mater.* **2005**, *17*, 77.
[19] G. H. Chen, W. G. Wang, C. L. Wu, J. R. Lu, P. P. Wang, X. F. Chen, *Carbon* **2004**, *42*, 753.
[20] G. H. Zheng, J. S. Wu, W. P. Wang, C. Y. Pan, *Carbon* **2004**, *42*, 2839.
[21] H. Kaczmarek, A. Podgorski, *Polym. Degrad. Stab.* **2007**, *92*, 939.
[22] Z.-M. Dang, Y.-H. Lin, C.-W. Nan, *Adv. Mater.* **2003**, *15*, 1625.
[23] J. G. Meier, J. W. Mani, M. Kluppel, *Phys. Rev. B* **2003**, *15*, 1625.
[24] C. W. Nan, *Prog. Mater. Sci.* **1993**, *37*, 1.
[25] Z. M. Dang, B. Peng, D. Xie, S. H. Yao, M. J. Jiang, J. B. Bai, *Appl. Phys. Lett.* **2008**, *92*, 112910.
[26] S. H. Xie, Y. Y. Liu, Y. J. Li, *Appl. Phys. Lett.* **2008**, *92*, 243121.